Catalysis Science & Technology

ROYAL SOCIETY OF CHEMISTRY

PAPER

View Article Online
View Journal | View Issue

Cite this: *Catal. Sci. Technol.*, 2021, 11, 2497

A combined experimental and computational study to decipher complexity in the asymmetric hydrogenation of imines with Ru catalysts bearing atropisomerizable ligands†

Félix León,‡[a] Aleix Comas-Vives,[b] Eleuterio Álvarez[a] and Antonio Pizzano*[a]

$RuCl_2$(P–OP)(N–N) complexes (**1**) containing an atropisomerizable phosphine–phosphite (P–OP) and a chiral C_2 symmetric diamine (N–N) are readily prepared as *trans* isomers by successive addition of P–OP and N–N ligands to $RuCl_2(PPh_3)_3$. For these complexes, fast atropisomerization of the biaryl fragment at room temperature has been observed. Compound *trans*-**1a** cleanly isomerizes into a mixture of *cis* isomers in EtOH upon heating. DFT calculations reproduce accurately the ratio of isomers observed as well as the greater thermodynamic stability of the *cis* isomers of **1a**. Complexes **1** are efficient catalyst precursors for the asymmetric hydrogenation of *N*-aryl imines **5** in toluene under very mild conditions using KO^{t}Bu as a base (4 bar H_2, room temperature, **5**/**1**/KO^{t}Bu = 500/1/10). Among the catalyst precursors, **1f** provides good enantioselectivities in the hydrogenation of a wide range of *N*-aryl imines (84–96% ee, 16 examples). From DFT calculations, a mechanism consisting in stepwise transfer of a hydride and a proton from the dihydride to the imine has been proposed, with the most favourable paths for *R* and *S* products involving *cis*-dihydrides **d1R** and **d3S**, respectively. Among several hydrogen activation pathways examined in the *pro-R* route, the most favorable one consists of hydrogen coordination to a Ru–amido/amine adduct, followed by amine assisted activation of dihydrogen.

Received 14th December 2020,
Accepted 21st January 2021

DOI: 10.1039/d0cy02390f

rsc.li/catalysis

Introduction

Chiral Ru complexes bearing P- and N-ligands constitute a group of catalysts of paramount importance in the area of asymmetric hydrogenation.[1] Fueled by the seminal discovery by Noyori and coworkers about the outstanding performance of complexes containing BINAP and DPEN or DAIPEN ligands in the asymmetric hydrogenation of ketones,[2] the field has grown impressively and a vast diversity of catalysts comprising different combinations of ligands can be found in the literature.[3] Moreover, these types of catalysts have displayed a broad substrate scope for catalytic hydrogenation beyond ketones, which includes imines, esters, and amides, among others.[4]

The study of the mechanism of the prototypical asymmetric hydrogenation of ketones with the aforementioned catalysts has deserved considerable attention as well.[5] From this background, it is concluded that the ketone is reduced by an octahedral dihydride, generated in the reaction medium from a dihalo or a halo-hydride complex by the action of a base and hydrogen,[5a–c] by an outer sphere pathway. In this regard, computational studies by Dub and Gordon have shown the prevalence of a stepwise mechanism over a concerted one.[6] Another key mechanistic aspect regards the stereochemistry of the reducing dihydride. Due to their octahedral geometry, several isomers are possible depending on the nature of the ancillary ligands. It is worthy to note that *cis* isomers possess an additional source of chirality due to a stereogenic center located at the metal.[7] In this context, a detailed study by Morris and coworkers on the $Ru(H)_2(PPh_3)_2$((*R*,*R*)-dach) complex (**A**, Fig. 1) has shown that the *trans*,*cis* isomer is the active catalyst in the hydrogenation of acetophenone, while the *cis*, *cis* isomers (two isomers differing in metal configuration;

[a] *Instituto de Investigaciones Químicas and Centro de Innovación en Química Avanzada (ORFEO-CINQA), CSIC and Universidad de Sevilla, Avda Américo Vespucio 49, 41092 Sevilla, Spain. E-mail: pizzano@iiq.csic.es*
[b] *Department of Chemistry, Universitat Autònoma de Barcelona, 08193 Cerdanyola del Vallès, Catalonia, Spain*

† Electronic supplementary information (ESI) available: Experimental details of the synthesis and characterization of Ru complexes and procedures for asymmetric hydrogenation reactions. X-ray crystallographic data for **1a**, **1c**, **1i** and *cis*-**1a** and computational details. CCDC 2045798 (**1a**), 2045799 (**1c**), 2045800 (**1i**), 2045801 and 2045802 (*cis*-**1a**). For ESI and crystallographic data in CIF or other electronic format see DOI: 10.1039/d0cy02390f

‡ Present address: Nanyang Technological University, Singapore.

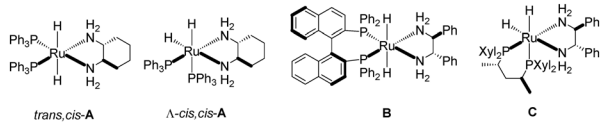

Fig. 1 Structures of *cis* and *trans* dihydride isomers relevant in the catalytic hydrogenation of ketones and imines.

only the Λ isomer is shown) are precursors of the active one.[5c] Aligned with these observations, mechanistic studies on $Ru(H)_2$((*S*)-BINAP)((*S*,*S*)-DPEN) (**B**) have considered the *trans* isomer as the competent catalyst.[5h] It is pertinent to note that Ohkuma and coworkers have otherwise proposed a *cis* dihydride catalyst in the asymmetric hydrogenation of imines catalyzed by *cis*-$Ru(Br)_2$((*S*,*S*)-Xyl-skewphos)((*S*,*S*)-DPEN) (**C**).[8] In connection with this, it should also be noticed that *cis* dichloro complexes based on diphosphine and amino-pyridine ligands are also effective in the asymmetric transfer hydrogenation of ketones.[9]

Following our interest in the application of chiral phosphine–phosphites (P–OP) in hydrogenation reactions, we preliminarily described the application of $Ru(Cl)_2$(P–OP)(DPEN) complexes (Fig. 2) in the enantioselective hydrogenation of *N*-aryl imines.[10a] Compared to ubiquitous diphosphine catalysts, the presence of a phosphite fragment in these complexes may have a profound influence in the catalytic system due to its π-acidity. Comparison between structures of the $Ru(Cl)_2$(P–OP)(DPEN) complexes showed that both *cis* and *trans* isomers can be formed depending on the structure of the P–OP ligand. Moreover, a remarkable feature of this catalytic system is that high levels of enantioselectivity were achieved with P–OP ligands bearing atropisomerizable phosphite fragments.[10a] This is an intriguing observation considering the complexity of the system, as the combination of two different phosphorus functionalities, the access to both *cis* and *trans* isomers and the atropisomerizable phosphite fragment can lead up to ten dihydrides with potential catalytic reactivity. In this contribution, we present a combined experimental and computational study on this catalytic system which explains the high levels of observed enantioselectivity. In addition, catalyst screening covering diverse combinations of P–OP and diamine ligands has detected a practical and versatile catalyst with the DPEN diamine as the sole chiral ligand, capable of reducing a variety of *N*-aryl imines under very mild conditions with good levels of activity and enantioselectivity.

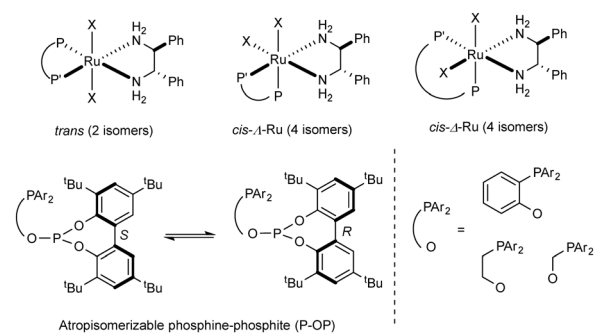

Fig. 2 Structures of the *trans* and *cis* stereoisomers of $Ru(X)_2$(P–OP)((*S*,*S*)-DPEN) (X = Cl, H; for the number of isomers, it should be considered that there are two possible configurations of the atropisomerizable biaryl phosphite; P and P′ denote either a phosphine or a phosphite fragment).

Results and discussion

Synthesis and structural features of $Ru(Cl)_2$(P–OP)(N–N) complexes

$Ru(Cl)_2$(P–OP)(N–N) complexes (**1a–1k**, Scheme 1) were prepared in a one-pot reaction by successive addition of phosphine–phosphite and diamine ligands to $RuCl_2(PPh_3)_3$. Monitoring the reactions by $^{31}P\{^1H\}$ NMR showed the formation of one set of signals, enabling the isolation of compounds **1** with moderate to high yields (56–76%). This procedure thus constitutes a substantial improvement over the reaction of $Ru(2\text{-Me-}C_3H_4)_2$(P–OP) with HCl and diamine used by us before,[10] which led to complexes **1** as diastereomeric mixtures with rather low yields (*ca.* 10–40%). In the case of complexes **1a–1c**, characterized by an oxamethylene backbone, the undesired formation of $Ru(Cl)_2(P\text{–}OP)_2$ was observed. Latter complexes are characterized by triplets in the phosphine and phosphite regions in the $^{31}P\{^1H\}$ NMR spectra (*e.g.* centred at 133.0 and 4.5 ppm, $^2J_{PP}$ = 37 Hz, in the synthesis of **1c**). These by-products result from the reaction of $RuCl_2$(P–OP)(PPh_3) with P–OP and better yields of **1a–1c** were obtained in more diluted reactions. The procedure in Scheme 1 is rather versatile and allowed us to introduce several chiral 1,2-diaryl-1,2-ethanediamines (**3a–3d**) or a 1,2-diisopropyl derivative (**4**) as well as P–OP ligands differing in their backbone structure. In the search for chirally-economic catalysts,[9b] an atropisomerizable biaryl fragment in the P–OP ligand has been maintained as a common element[11] in the library of catalysts. The exploitation of such an element is a rather powerful strategy in the design of chiral catalysts as it generates a stereogenic axis from an achiral ligand upon coordination, with its configuration being potentially controlled by a chiral ancillary ligand.[12] For instance, this approach has been applied successfully in Ru hydrogenation catalysts by the combination of chiral diamines (*e.g.* DPEN) and atropisomerizable diphosphines.[12a,b,e]

The structure of some representative complexes **1** was then examined by X-ray crystallography. It should be recalled that the preliminary structure determination of complex **1d** displayed the presence of two diastereomeric structures with a *trans* stereochemistry, differing in the configuration of the biaryl fragment.[10a,13] Analysis of complex **1i** showed an analogous pattern (Fig. 3a), as well as **1a** and **1c** (see the ESI†). This stereochemistry seems associated with the synthetic route in Scheme 1 and can reasonably be assumed for the rest of complexes **1**. To avoid redundancy, an explicit mention of the *trans* stereochemistry of **1** will only be made

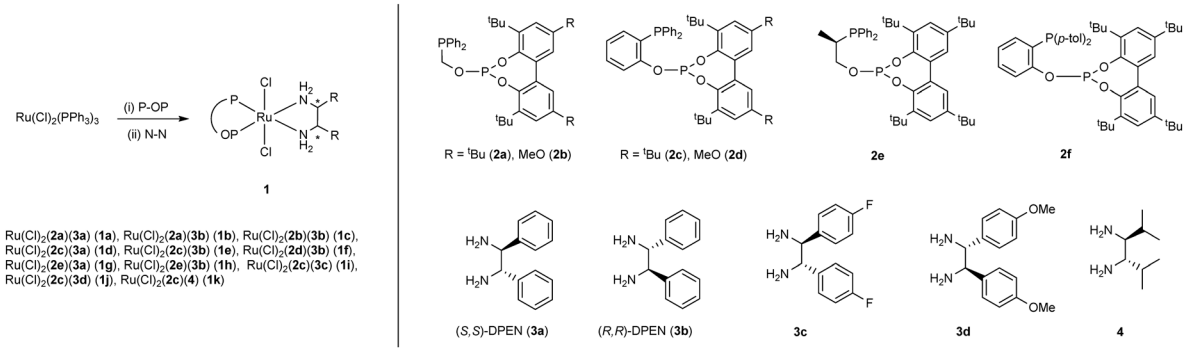

Scheme 1 Synthesis of complexes **1**.

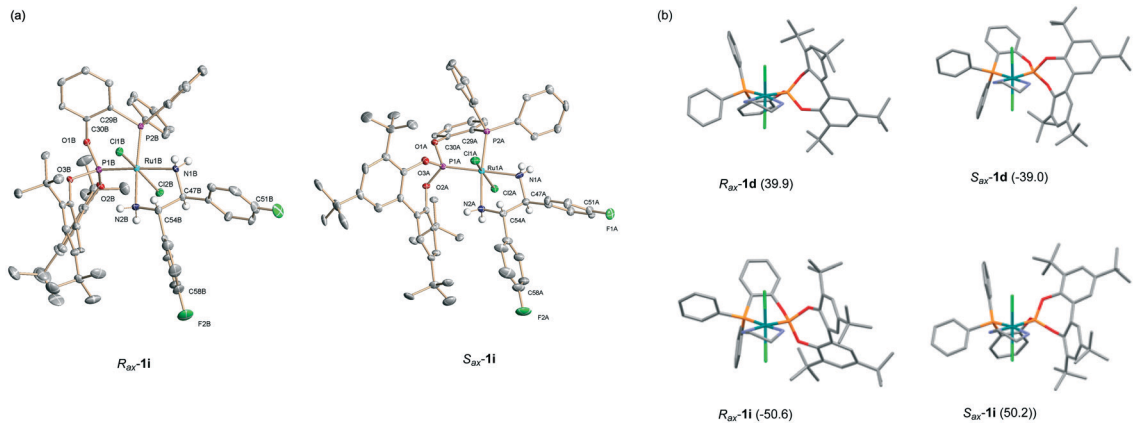

Fig. 3 ORTEP views of the R_{ax} and S_{ax} diastereomers of complex **1i** observed in the crystal lattice (a; hydrogen atoms have been omitted for clarity). Comparison of structures of the diastereomers of complexes **1d** and **1i** (b; numerical values correspond to the P_O–Ru–P_C–C_{Ar} dihedral angles in degrees; P_O and P_c denote the phosphorus atoms of phosphite and phosphine fragments, respectively, while C_{Ar} corresponds to the backbone aryl carbon bonded to P_C; diamine aryl substituents and hydrogen atoms have been omitted for clarity).

in selected cases for the sake of clarity. The change in the configuration of the stereogenic axis is accompanied by an extensive conformational change of the P–OP ligand backbone and of the arrangement of the phenylphosphine substituents, in such a way that both structures would be mirror images if the diamine backbone were not considered.[13b] Another common feature of these structures is that the axial hydrogens of amino groups display a hydrogen bond with an adjacent chloro ligand,[14] as the corresponding distances range between 2.7 and 2.8 Å, while the sum of van der Waals radii lies between 2.9 and 3.0 Å.[15] Moreover, these axial hydrogens exhibit a *syn* periplanar orientation with chloro ligands, with torsion angles ranging between *ca.* 13 and 22 degrees. Finally, an interesting difference between structures of complexes **1d** and **1i** regards the different orientation of the phenylene backbone fragment with regard to the phosphite biaryl moiety as shown by the opposite signs of the values of the P_O–Ru–P_C–C_{Ar} dihedral angle (Fig. 3b) in the R_{ax} and S_{ax} diastereomers.

According to the presence of two diastereomers of complexes **1** in the crystal lattice, the observation of one set of signals in $^{31}P\{^1H\}$ NMR at room temperature agrees with the fast atropisomerization of the biaryl moiety.[16] Confirmation of the existence of a dynamic process comes from variable temperature $^{31}P\{^1H\}$ NMR spectroscopy of **1b** (Fig. 4), which shows the existence of two species in a 3 : 1 ratio at −90 °C, characterized by doublets in the phosphine and phosphite regions (major: 174.5, 69.5 ppm; minor: 175.4, 67.6 ppm) with a coincident value of $^2J_{PP}$ coupling constants (47 Hz). Coalescence of signals was observed at around −70 °C, while over −50 °C, two sharp doublets were observed. For this dynamic process, a free activation energy of 9.2 kcal mol^{-1} was determined at the coalescence temperature by lineshape analysis, while an analogous analysis for **1d** gave a value of 10.2 kcal mol^{-1} (coalescence temperature −65 °C, see the ESI† for details).

Pertinent to note in this context, Ohkuma and coworkers have observed that a mixture of *cis* and *trans* isomers of Ru(Br)$_2$((*S*,*S*)-Xyl-skewphos)((*S*,*S*)-DPEN) can be converted into the *cis* isomer by treatment with a ^{i}PrOH/CH_2Cl_2 mixture. The aforementioned allyl route led to a mixture of isomers of Ru(Cl)$_2$(**2a**)(**3a**) composed of *trans* complex **1a** and additional isomers. From this mixture, a *cis* isomer could be characterized by X-ray diffraction (*cis*-**1a**; *cis*-**1** type structure,

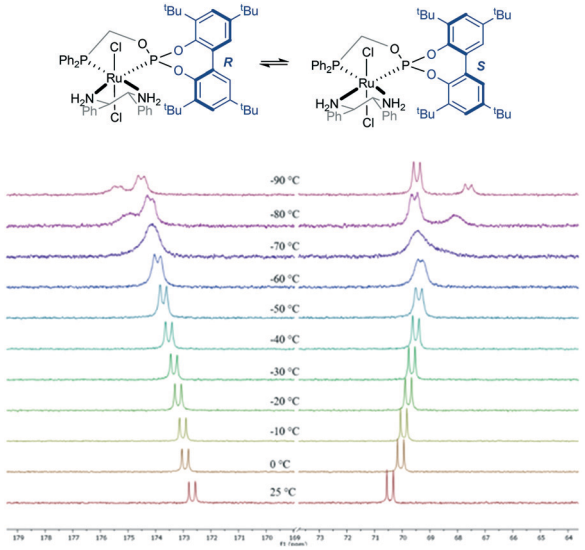

Fig. 4 $^{31}P\{^1H\}$ NMR spectra of **1b** registered at several temperatures.

R_{ax} configuration; see Fig. 5a in the Computational studies section).[10b] According to this finding, we have examined the isomerization of *trans* complex **1a** in alcoholic solvents. Interestingly, heating a solution of this complex in EtOH for 16 h at 60 °C leads to a mixture of two new species in a 2.5 : 1 ratio with almost complete conversion (95%). These compounds are characterized by very similar NMR data and among them, an upfield shift of resonances of NH signals with respect to those of the starting *trans* complex can be remarked, attributable to the proximity of the biaryl phosphite moiety to the amino fragments and hence indicative of a *cis* structure. From the mixture, it was possible to crystallize the major isomer which was identified as *cis*-**1a** by X-ray analysis (minor *cis* isomer will be denoted as *cis*-**1a′**). In contrast, **1d** is rather unreactive under these reaction conditions and only a conversion of 10% could be observed after 3 days at 70 °C in an EtOH–1,2-dichloroethane (1 : 1) mixture, exhibiting two new species in a *ca.* 3 : 1 ratio by $^{31}P\{^1H\}$ NMR.

Catalytic studies

In our preliminary study of the hydrogenation of imine **5a** with $Ru(Cl)_2$(P–OP)(N–N) complexes (Scheme 2), we screened several reaction conditions.[10a] Among them, the best results were obtained under very mild conditions in toluene with $Ru(Cl)_2$(**2f**)(**3a**) (4 bar H_2, RT, S/C/KO^{t}Bu = 500/1/10, full conversion in 24 h; 93% ee). Examination of the performance of the series of catalyst precursors **1** under these reaction conditions (Table 1) showed near complete reactions with the only exception of **1c** (86%, entry 3) and particularly **1k**, for which a poor value was observed (27%, entry 10). Moreover, good values of enantioselectivity were obtained (89–95% ee), with **1a** and **1f** surpassing the *p*-tolyl catalyst (entries 1 and 5, respectively). The uniformly high levels of enantioselectivity with complexes **1** also demonstrate that the atropisomerizable phosphite fragment is a valuable element for the design of chirally economic catalysts. It is worth noting that no influence of the electronic properties of DPEN substituents was observed with catalyst precursors **1i** and **1j** (entries 8 and 9). For the couple of diastereomeric complexes **1g** and **1h**, little matching/mismatching effects were observed, with a small difference of enantioselectivity between them and the configuration of the product determined by that of DPEN (entries 6 and 7). This is general and for catalyst precursors bearing (*S*,*S*)-diamines, the *R* product is formed (and conversely the *S* product from (*R*,*R*)-diamines). Among the complexes examined, **1f** showed the best performance with a complete conversion and 95% ee. From this satisfactory result, we next screened the application of this complex in the hydrogenation of a set of *N*-aryl imines derived from aryl alkyl ketones (**5b**–**5o**). For these substrates, full conversion and enantioselectivities between 84 and 96% ee were observed (Table 2). It is worth

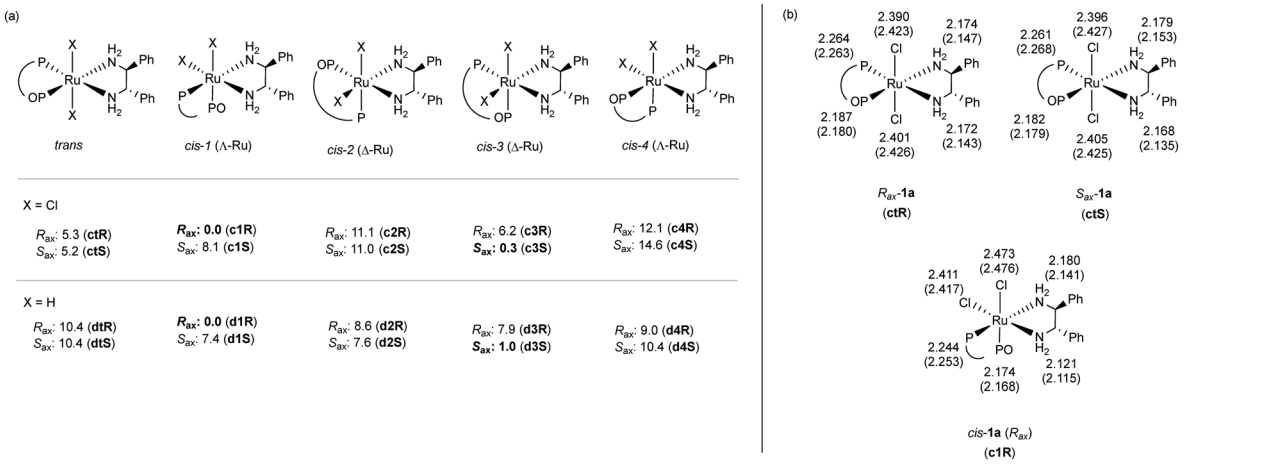

Fig. 5 Relative free energies calculated for isomers of $Ru(Cl)_2$(**2a**)(**3a**) and $Ru(H)_2$(**2a**)(**3a**) (a; ΔG in kcal mol^{-1}, notation in brackets). Ru ligand bond distances determined by X-ray crystallography and computed (in brackets) for stereoisomers of $Ru(Cl)_2$(**2a**)(**3a**) (b).

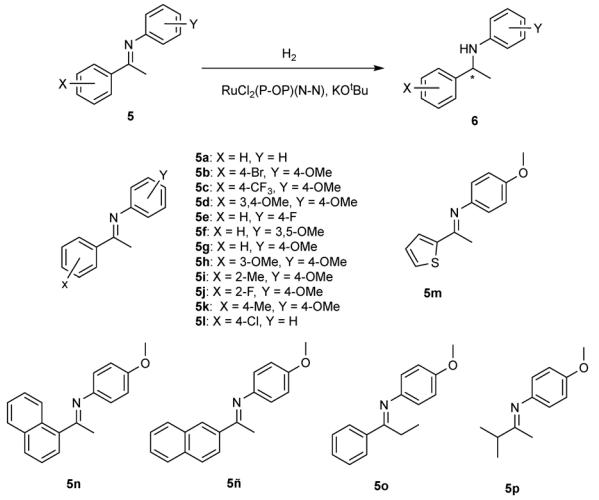

Scheme 2 Catalytic hydrogenation of imines **5**.

Table 1 Hydrogenation of imine **5a** with catalyst precursors **1**[a]

Entry	Cat	Conv (%)	ee (%; config)
1	**1a**	100	94 (*R*)
2	**1b**	100	94 (*S*)
3	**1c**	86	90 (*S*)
4	**1e**	100	92 (*S*)
5	**1f**	100	95 (*S*)
6	**1g**	100	89 (*R*)
7	**1h**	100	93 (*S*)
8	**1i**	100	90 (*R*)
9	**1j**	95	90 (*S*)
10	**1k**	27	nd

[a] Reactions performed under 4 bar H_2 in toluene at room temperature for 24 h with KO^{t}Bu as a base; S/C/B = 500/1/10; conversion was determined by ^{1}H NMR. % ee determined by HPLC. Configuration was determined by comparison with literature data.[17]

Table 2 Hydrogenation of imines **5b–5o** with catalyst precursor **1f**[a]

Entry	Imine	% ee (conf)
1	**5b**	94 (*S*)
2	**5c**	94 (*S*)
3	**5d**	87 (*S*)
4	**5e**	94 (*S*)
5	**5f**	91 (*S*)
6	**5g**	96 (*S*)
7	**5h**	95 (*S*)
8	**5i**	93 (*S*)
9	**5j**	95 (*S*)
10	**5k**	94 (*S*)
11	**5l**	91 (*S*)
12	**5m**	95 (*S*)
13	**5n**	84 (*S*)
14	**5ñ**	92 (*S*)
15	**5o**	96 (*S*)

[a] Reactions performed under 4 bar H_2 in toluene at room temperature for 24 h with KO^{t}Bu as a base; S/C/B = 500/1/10; full conversion (^{1}H NMR) was observed in all reactions. % ee determined by HPLC. See the ESI† for determination of configuration.

noting that the set includes demanding *ortho* substituted imines (entries 8 and 9), naphthyl imines (entries 13 and 14) and a thienyl example (entry 12). In contrast, no conversion was observed in the hydrogenation of challenging isopropyl methyl imine **5p**.

To examine the practical character of **1f**, we have also prepared for the gram scale hydrogenation of **5h** (Scheme 3), as the resulting product has attracted interest in the synthesis of the NPS R-568 calcimimetic.[18] We were pleased to note that a reaction using 2.0 g of **5h** at S/C/B = 1000/1/10 led to full conversion in 24 h, yielding amine **6h** with 96% isolated yield and 95% ee.

Detailed mechanistic studies by the group of Noyori have shown that hydride–borohydride complexes Ru(H)(BH_4)(tol-BINAP)(1,2-diamine) (1,2-diamine = DPEN, en, DAIPEN) are suitable catalyst precursors for the hydrogenation of ketones in isopropanol without the need of an additional base,[19,20] while no catalytic activity was observed in toluene.[5b] Based on this background, we have prepared Ru(H)(BH_4)(**2c**)(**3b**) (**7**) by treating **1e** with an excess of $NaBH_4$ in a toluene : EtOH (1 : 1) mixture (Scheme 4).[21] An analysis by NMR of the product showed the existence of two isomers of **7** in a 7 : 3 ratio. A 2D NOESY experiment with the mixture indicates that the major isomer possesses a *trans* stereochemistry, while the minor one, attending to the similarity between the spectroscopic data of both species, can be assigned as the alternative *trans* isomer. We have next analysed the performance of **7** in the hydrogenation of **5a** in the absence of a base. First, no reaction was observed in toluene, in accord with the literature precedent mentioned above. On the other hand, a reaction performed under 20 bar H_2 in ^{i}PrOH and 60 °C with an S/C = 100 showed a complete conversion and 84% ee after 24 h. For comparison, a reaction prepared with **1e** under the same reaction conditions but with addition of a small amount of KO^{t}Bu to guarantee catalyst activation (S/C/B = 100/1/5) provided 91% conversion and 83% ee. These results point to a common enantiodetermining step starting from **1e** and KO^{t}Bu or **7** in isopropanol. These observations are analogous to those reported for the BINAP/DPEN system in the asymmetric hydrogenation of acetophenone.[5b]

In addition, we have examined the hydrogenation of **5g** under our standard conditions with *trans* complex **1a**, with the mixture of *cis*-**1a** and *cis*-**1a′** isomers (resulting from isomerization of **1a**) and with *cis*-**1a** (obtained by crystallization of the latter mixture). Full conversion and coincident enantioselectivities (94.2, 94.2 and 94.6% ee, respectively) were observed in the three reactions, pointing to

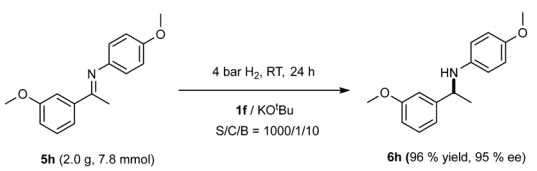

Scheme 3 Gram scale synthesis of **6h**.

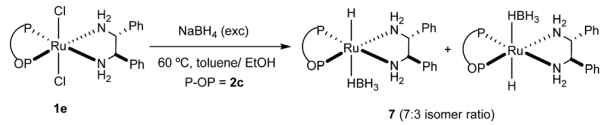

Scheme 4 Synthesis of hydride borohydride **7**.

the same catalyst formed independently of the stereochemistry of the catalyst precursor.

It is worth noting in this context that Bäckvall and coworkers reported the racemization of some enantiopure amines **6** in toluene at 110 °C using the Shvo catalyst and 0.5 equivalents of 2,4-dimethyl-3-pentanol, with the racemization rate being significantly reduced when the reaction temperature was lowered.[22a] Moreover, in the presence of a hydrogen acceptor, imines **5** could be obtained.[22b] Based on this background, it seems highly interesting to examine if the formation of amines **6** is irreversible in the present catalytic system. To this aim, the hydrogenation of **5g** using **1a** under standard reaction conditions was stopped at 25% conversion. This reaction showed a 93.4% ee, which is very close to the value obtained at full conversion (94.2% ee). In addition, a sample of *rac*-**6g** was exposed to catalytic reaction conditions for 24 h and neither a variation of the enantiomeric ratio nor imine were observed. To discard the idea that any impurity could inactivate the catalyst generated from **1a** in the latter experiment, a complementary one using a mixture of **5g** and *rac*-**6g** (1 : 3.4) was examined under the same reaction conditions. After 24 h, complete reduction of the imine was observed and determination of the enantioselectivity of **6g** gave a value of 20.8% ee. For this experiment, a theoretical value of 21.2% ee can be estimated if the imine were hydrogenated with a 93% ee. These results therefore indicate that no reversibility of the reduction step should occur under the mild catalytic conditions used.

Computational studies

We subsequently did computational studies to complement the experimental results *via* DFT-based methods.[23] These comprise the structural and stereochemical features of complex **1a** as well as the study of the mechanism of a representative imine hydrogenation reaction, with the aim of understanding the role of the atropisomerizable phosphite fragment and the high enantioselectivities observed. In addition, some studies regarding **1d** and the corresponding dihydride will be included for comparative purposes. As mentioned, outer sphere reduction by Ru(H)$_2$(diphosphine)(diamine) is a well-established step in the asymmetric hydrogenation of ketones in both protic and aprotic solvents.[5] Moreover, due to the similarity between the Ru catalyzed hydrogenation of imines and ketones,[1b] some catalysts have been proposed to reduce imines enantioselectively following an outer sphere mechanism,[4a,b,8] although no detailed computational study has been provided. In this regard, results of reactions performed with **1a** and **7** in isopropanol point to an outer sphere reduction of **5a** by Ru(H)$_2$(**2a**)(**3a**) as the enantioselective step. Although the nature of the resting catalyst state in toluene and isopropanol should be different,[5b] it is reasonable to assume that this reduction mode should also operate in toluene.[24]

Structure and stereochemical features of Ru(Cl)$_2$(2a)(3a) and Ru(Cl)$_2$(2c)(3a). The structures of isomers of dichloro complex **1a** have been optimized to get a deeper insight into their relative stabilities (Fig. 5a). A good agreement has been observed between the calculated structures of **c1R**, **ctR** and **ctS** and the X-ray determined structures of *cis*-**1a**, and R_{ax} and S_{ax} diastereomers of *trans* complex **1a**, respectively (Fig. 5b). Moreover, **ctR** and **ctS** are very close in energy, as could be expected from the behaviour shown by **1a** in solution. On the other hand, **c1R** and **c3S** are more stable than the *trans* structures, in good agreement with the observed isomerization of **1a**. In addition, the small difference in free energy between **c1R** and **c3S** gives a 1.7 : 1 calculated ratio, which is in good agreement with the ratio of ***cis*-1a** and *cis*-**1a′** species observed after the isomerization. Finally, **c1R** shows the same stereochemistry as that of the predominant *cis* isomer in solution (*cis*-**1a**), while the minor one (*cis*-**1a′**) should have the structure shown by **c3S**.

A remarkable result regards differences in energy between *cis* structures differing in the configuration of the phosphite stereogenic axis. Thus, low to negligible differences are observed between atropisomers of types *cis*-**2** and *cis*-**4**, which contain the phosphite fragment coordinated in a *cis* position to one NH_2 group. In contrast, there are considerable energy differences between atropisomers of types *cis*-**1** and *cis*-**3**, characterized by a phosphite *cis* to both NH_2 groups in an arrangement which favors the interaction between the biaryl phosphite and the diamine backbone. Most interestingly, the preferred biaryl configuration depends on that of the metal, with **c1R** and **c3S** being appreciably more stable than their respective atropisomers **c1S** and **c3R**, with free energy differences of 8.1 and 5.9 kcal mol^{-1}, respectively.

Moreover, we have examined selected structures for complex **1d**. Initially, examination of *trans* structures with the backbone orientation shown by X-ray analysis leads to a couple of diastereomers (**ctR′** and **ctS′**) structurally very close to the experimental structures, with a minimal free energy difference between them (0.4 kcal mol^{-1}). In addition, structures with a backbone orientation shown by **1i** were also investigated. Notably, the corresponding *trans* diastereomers (**ctR″** and **ctS″**) were appreciably more stable than **ctR′** and **ctS′**, with free energy differences of 4.5 and 5.6 kcal mol^{-1}, respectively. Among the four isomers, **ctS″** is the more stable one, with the **ctR″** isomer being 1.5 kcal mol^{-1} higher in free energy than the former species. Presumably, easy interconversion between the four conformers should occur in solution, while the observation of less stable conformers of **1d** by X-ray crystallography should be caused by a better packing in the crystal lattice. On the other hand, a comparison between *cis*-**1**-*R* and *cis*-**3**-*S* type structures for **1d** (**c1R′** and **c3S′**, respectively) shows a higher stability for the

former species (1.6 kcal mol^{-1} in free energy). However, these *cis* structures are slightly less stable than **ctS″**, with free energy differences of 0.4 and 2.0 kcal mol^{-1}, respectively. Therefore, the comparison of energies of isomers **1a** and **1d** indicates that the *cis*/*trans* preference in dichloro complexes is rather sensitive to the precise structure of the phosphine–phosphite ligand.

In addition, the atropisomerization of **1a** has also been studied (Fig. 6). As mentioned, this dynamic process involves a conformational change not only in the biaryl moiety, but also in the backbone and in the position of the phosphine substituents. Starting from **ctR**, which is characterized by a biaryl dihedral angle (φ) of −49.1°, a scan of the reduction of this parameter allowed us to locate a transition state (**atrop-TS1**, φ = 1.9°) lying 9.3 kcal mol^{-1} in free energy above **ctR**. This transition state leads to an alternative conformer (**conf-1**, ΔG = 5.2 kcal mol^{-1}) characterized by a value of 28.3° for φ, and thus displaying the S_{ax} configuration. To complete the dynamic process to reach **ctS**, a pathway involving two additional transition states and two conformers has been found (see the ESI† for further details). Notably, the highest point along the whole atropisomerization pathway corresponds to **atrop-TS1**, in good agreement with the experimental value obtained by VT-NMR for the energy barrier of the fluxional process shown by **1a**.

Dihydrides. The differences in free energy between isomers of Ru(H)$_2$(**2a**)(**3a**) (Fig. 5a) parallel the trend observed for those of the dichloro complex. Hence, **d1R** and **d3S** are the more stable dihydrides of the series, while the *trans* isomers are among the less stable ones. In addition, compounds **d1R** and **d3S** have appreciably lower free energies than their corresponding atropisomers (7.4 and 6.9 kcal mol^{-1}, respectively). Moreover, variations in Ru–H distances are in good accord with the *trans* influence of ancillary ligands.[25] Thus, those of the *trans* dihydrides are in the 1.679–1.685 Å range, while for the hydride ligands *trans* to the phosphite, phosphine and amino ligands, ranges of 1.657–1.670, 1.648–1.658 and 1.602–1.615 Å are observed, respectively. Examination of selected structures of stereoisomers of Ru(H)$_2$(**2c**)(**3a**) (*i.e.* those corresponding to **1d**) showed a similar stability pattern to that shown above, with the *cis*-**1**-R_{ax} type isomer (**d1R′**) as the most stable one, while the *cis*-**3**-S_{ax} type structure (**d3S′**) is only 0.1 kcal mol^{-1} in free energy over **d1R′**. These *cis* structures are more stable than the *trans* isomers irrespective of the backbone conformation of ligand **2c**. Thus, structures **dtR′** and **dtS′** are 6.6 and 7.1 kcal mol^{-1} above **d1R′** in free energy, while **dtR″** and **dtS″** are 3.9 and 4.2 kcal mol^{-1} higher than **d1R′**, respectively. For these structures, the Ru–H distances follow the trend commented above and have value ranges of 1.675–1.684, 1.658–1.663 and 1.605–609 Å for hydrides *trans* to the hydride, phosphite and amino ligands, respectively. These values indicate that the significantly higher reactivity of *trans* dihydrides, compared to *cis* ones, characteristic of the well-studied diphosphine catalysts,[5b,h] may not be transferable to the present system due to the phosphite fragment. Thus, the *cis*-**1** and *cis*-**3** dihydrides may have comparable reactivities to the *trans* isomers.

Amido–hydride complexes. Another kind of important complexes in the catalytic system are amido–hydride complexes Ru(H){(*S*,*S*)-NH–CHPh–CHPh–NH$_2$}(**2a**).[5c] These compounds should be formed by the activation of Ru(Cl)$_2$(**2a**)(**3a**) with a base and hydrogen as well as by the reduction of the imine by Ru(H)$_2$(**2a**)(**3a**) (see below). Conversely, the reaction of amido–hydrides with hydrogen should lead to dihydrides Ru(H)$_2$(**2a**)(**3a**). Considering that the latter reaction can occur with small structure rearrangement, the starting structures for amido–hydride compounds can be generated by the formal abstraction of a hydride and a pseudo-axial adjacent amine proton from the dihydrides.[5a] By optimization of these starting structures, either distorted trigonal bipyramidal or square pyramidal species were located, with those of the former type being significantly more stable than the latter (*ca.* 30 kcal mol^{-1} in free energy, see the ESI†). Amido and amino fragments of the deprotonated DPEN occupy the equatorial and apical

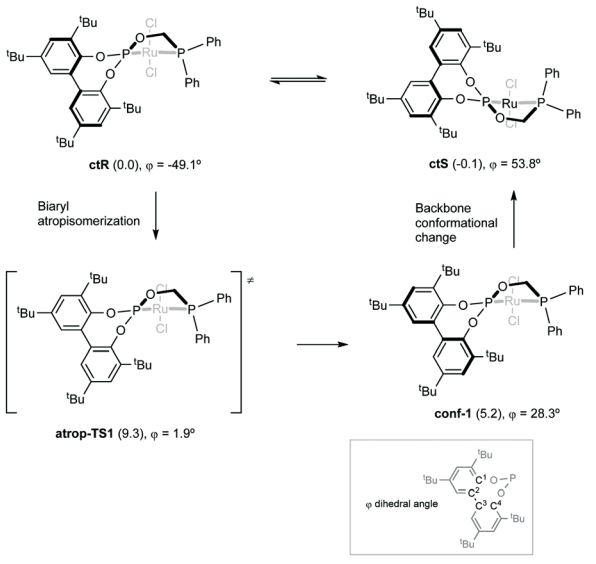

Fig. 6 Schematic fluxional mechanism computed for the atropisomerization of **1a** (relative free energies in kcal mol^{-1} in brackets relative to **ctR**; diamine ligand has been omitted for clarity).

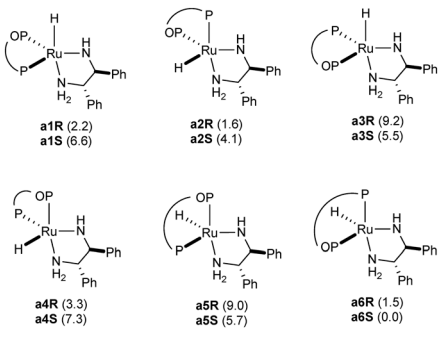

Fig. 7 Structures of amido–hydride complexes (ΔG relative to **a6S** in kcal mol^{-1} in brackets).

coordination positions in the bipyramidal complexes respectively (Fig. 7). In turn, no clear preference of the remaining ligands for an axial/equatorial position seems apparent. As expected, the Ru–amido bond distance is shorter than the Ru–amino one. For instance, for **a1R**, values of 1.970 and 2.221 Å have been obtained. For this structure, the equatorial plane is defined by the amido and P ligands, with N(amido)–Ru–P(phosphine) and N(amido)–Ru–P(phosphite) angles of 162.5 and 116.0 degrees, respectively. Finally, relatively small free energy differences are observed between the atropisomers of each type of amido–hydride (ΔG = 1.5–4.4 kcal mol^{-1}), if compared with the stabilization observed for **d1R** and **d3S** with regard to their atropisomers.

Imine reduction. An inspection of the structures of **d1R** and **d3S** indicates that the hydride located in the *trans* position to the amino group is surrounded by one phenyl substituent of the phosphine and one of the ^{t}Bu groups (Fig. 8a and b), thus blocking the approach of the imine C═N fragment to the corresponding Ru(H)–NH_2 moiety. As mentioned above, the Ru–H distances in the computed structures indicate an appreciably longer distance for the hydride *trans* to the phosphite in comparison with that *trans* to the amino ligand in **d1R** (1.670 *vs.* 1.604 Å) and **d3S** (1.666 *vs.* 1.604 Å). Based on these considerations, we have reasonably assumed an easier transference of the hydride *trans* to the phosphite from either **d1R** or **d3S** to **5a**, compared with that *trans* to the amine.

Considering the presence of two NH_2 groups in **d1R** (*trans* to phosphine or to hydride) and two prochiral faces of **5a**, four different approaches of the imine can be considered (Fig. 8c), as well as in the case of **d3S**. It is worth noting that the approximation of the substrate to the dihydride leads to the formation of loose precomplexes. Among the eight precomplexes, significant stabilization over their components is observed in the cases of **d1R-RP-5a** and **d3S-SP-5a**, with ΔG values of −7.1 and −7.0 kcal mol^{-1}, respectively. This stabilization can be ascribed to diverse substrate–ligand non-covalent interactions (NCI).[26] For instance, in the case of **d1R-RP-5a**, C–H/aryl interactions,[27] a high number of C–H/C–H dispersion interactions,[28] and a N···H–N interaction between the imine nitrogen and a NH fragment of the diamine ligand have been detected (Fig. 9). This NCI driven stabilization is a remarkable aspect for an outer-sphere mechanism, as these weak interactions enable structural preorganization[29] of the substrate–catalyst complex favoring the reduction.

From imine–dihydride precomplexes, the hydride transfer step to give monohydride–amide ionic pair species was next investigated. This class of transition states will be referred in the following as TS1. Among the TS1 transition states for **d1R** and **d3S** (Fig. 10), the most favorable one corresponds to *pro-R* precomplex **d1R-RP-5a** (**TS1-d1R-RP-5a**, $\Delta\Delta G^{\ddagger}$ = 0.0 kcal mol^{-1}; in the following, this transition state will be used as the reference to compare energies of TS1 transition states). The most favorable TS1 for the *S* enantiomer (**TS1-d3S-SP-5a**) involves **d3S** dihydride and has a $\Delta\Delta G^{\ddagger}$ value equal to 1.6 kcal mol^{-1} (see the ESI† for data on TS1 energies for the rest of the dihydride precomplexes). This is, moreover, the lowest TS1 transition state for **d3S** dihydride, followed by a *pro-R* one with $\Delta\Delta G^{\ddagger}$ = 4.9 kcal mol^{-1}. Despite **TS1-d1R-RP-5a** and **TS1-d3S-SP-5a** lying 6.2 and 7.8 kcal mol^{-1} in free energy above the corresponding dihydride imine precomplexes, they are very close in free energy to the starting dihydrides and free imine (−0.88 and 0.76 kcal mol^{-1} for **TS1-d1R-RP-5a** and **TS1-d3S-SP-5a** compared with **d1R** and free **5a**, respectively), due to the stabilization associated with the formation of the dihydride imine precomplexes.

Based on the literature precedents on the higher reactivity of *trans* dihydrides over *cis* ones[5] and considering that *trans*-dihydrides have the longest Ru–H bond distances in the series of Ru(H)$_2$(**2a**)(**3a**) dihydrides, it seems pertinent to study the barrier for the hydride transfer step for **dtR** and **dtS**. An inspection of these structures indicates that one of the hydride ligands is protected by a P–Ph and a ^{t}Bu group from the approach of the imine (views for **dtR** collected in

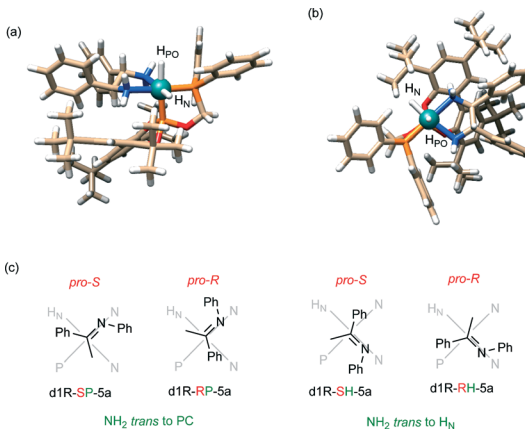

Fig. 8 Side (a) and top views (b) of **d1R** (H_{PO} and H_N denote hydrides *trans* to phosphite and amino ligands, respectively). Possible orientations of **5a** to **d1R** depending on the substrate face and NH_2 fragment approached (c).

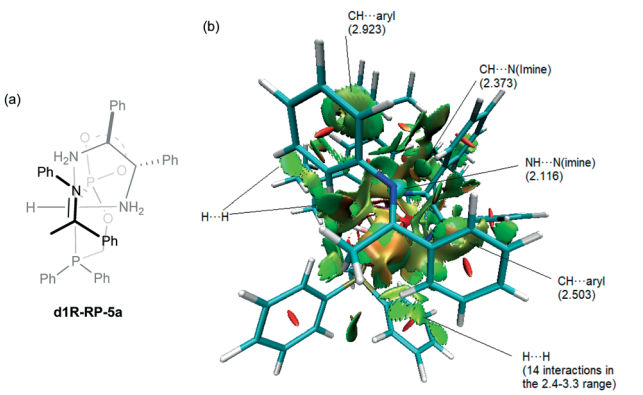

Fig. 9 **d1R-RP-5a** (a). Plot of non-covalent interactions for the latter precomplex (b, color ranges from strong attractive interactions in blue to strong repulsive ones in red; distances between interacting atoms or centroids of aryl rings in Å).[30]

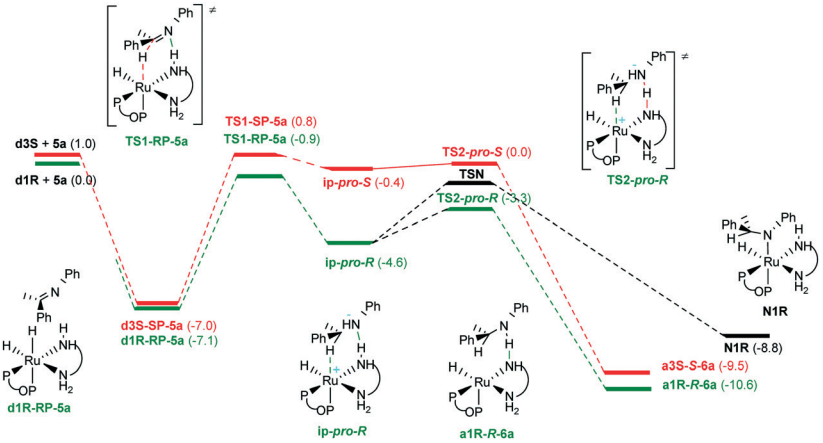

Fig. 10 General scheme for the reduction of imine **5a** (ΔG relative to **d1R** + **5a** in kcal mol^{-1} in brackets).

Fig. 11); therefore, participation of this hydride should only be possible after atropisomerization of the P–OP ligand (*i.e.* conversion of **dtR** in **dtS** and *vice versa*). Accordingly, only the transference of the less encumbered hydride needs to be examined for these dihydrides. As mentioned above for **d1R** and **d3S**, there are four possible imine approaches for both **dtR** and **dtS**, leading to eight precomplexes and corresponding TS1 transition states. For those leading to the *R* product, the $\Delta\Delta G^{\ddagger}$ values range between 3.9 and 18.2 kcal mol^{-1}, while for the *pro-S* ones, we found $\Delta\Delta G^{\ddagger}$ values that range between 8.7 and 18.6 kcal mol^{-1}. Presumably, steric effects associated with the bulky phosphite fragment in the equatorial plane should be responsible for the higher barriers observed for the *trans*-dihydrides. Likewise, an examination of the structures of dihydrides of types *cis*-**2** and *cis*-**4** indicates a substantial steric encumbrance around the hydride located in the *trans* coordination position to the phosphine ligand (*i.e.* that characterized by a longer Ru–H bond) because of the orientation of the biaryl phosphite, with the exception of **d2S**. For this dihydride, the corresponding set of four precomplexes was calculated, with **d2S-RP-5a** and **d2S-RH-5a** being already higher in free energy than **TS1-d1R-RP-5a** by 3.4 and 5.5 kcal mol^{-1}, respectively. On the other hand, **d2S-SH-5a** is 2.8 kcal mol^{-1} over **TS1-d3S-SP-5a**, while **d2S-SP-5a** is only 0.8 kcal mol^{-1} more stable in free energy than the latter transition state, with **TS1-d2S-SP-5a** being 11.8 kcal mol^{-1} higher in free energy than **TS1-d3S-SP-5a**. Considering that TS1 possess the highest free energy in the reduction pathway of **5a** by **d1R** and **d3S** (Fig. 10), the values of transition states of type TS1 for **d2S**, **dtR** and **dtS** point to *cis*-dihydrides **d1R** and **d3S** as the actual catalysts in the present system.

A remarkable feature of precomplexes **d1R-RP-5a** and **d3S-SP-5a** is that they show the substrate appropriately arranged for the hydride transfer step and a minimal structural variation from the precomplexes to the corresponding TS1 is required (Fig. 12). Moreover, **TS1-d1R-RP-5a** and **TS1-d3S-SP-5a** are stabilized by a hydrogen bond between the imine nitrogen and a N–H of the diamine, with N···H distances of

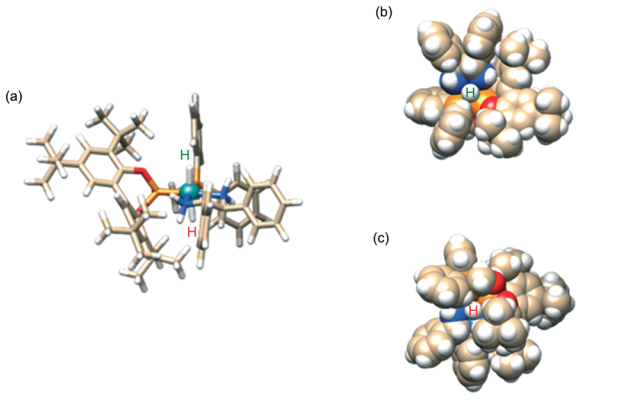

Fig. 11 Side view of **dtR** (a), and top (b) and bottom (c) space filling views of the same compound.

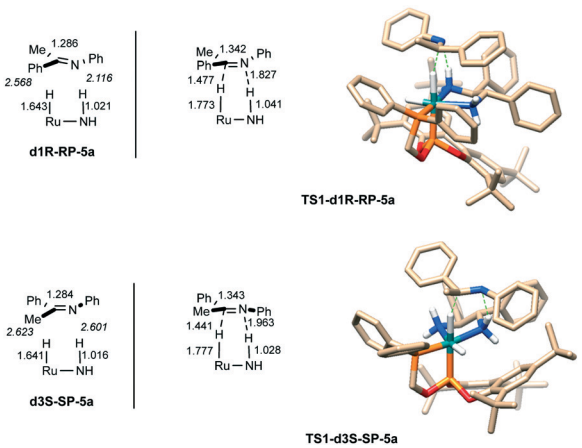

Fig. 12 Structures of the preferred *pro-R* (**TS1-d1R-RP-5a**, top right) and *pro-S* (**TS1-d3S-SP-5a**, bottom right) hydride transfer transition states (H atoms bonded to carbons have been omitted for clarity). Key structural distances involved in the transformation from dihydride–imine precomplexes to hydride-transfer transition states are given in Å in the corresponding schemes.

1.827 and 1.963 Å, respectively.[31] On the other hand, the distances between the hydride and the iminic carbon have values of 1.477 and 1.441 Å, respectively. In addition, expected elongations of the Ru–H and the C–N imine bonds are observed from the imine adducts to TS1 structures. In both transition states, the substrate displays a similar orientation, with the iminic nitrogen interacting with the amino ligand located in a *trans* coordination position to the phosphine, while the pseudoaxial Ph phosphine and the C–Ph imine substituents point to opposite directions.

The hydride transfer step from **TS1-d1R-RP-5a** and **TS1-d3S-SP-5a** next leads to ion pairs **ip-*pro-R*** and **ip-*pro-S***, respectively.[32] These species are stabilized by a hydrogen bond, with N···H distances of 1.788 Å and 1.821 Å for **ip-*pro-R*** and **ip-*pro-S***, respectively, as well as by an agostic interaction provided by the new C–H bond, with Ru–H distances of 2.031 Å and 2.033 Å, respectively. From the respective ion pair intermediates, a very easy proton transfer (TS2) *via* **TS2-*pro-R*** and **TS2-*pro-S*** can take place, lying 1.3 and 0.4 kcal mol^{-1} above the corresponding ion-pairs, respectively. The proton transfer step leads to adducts formed by an amido complex and enantiomers of amine **6a** (**a1R-*R*-6a** and **a3S-*S*-6a**, respectively). It is worth noting that this step also displays the completion of the hydride transfer step, as shown by a shortening of the corresponding C–H distance (*e.g.* from 1.201 Å in **ip-*pro-R*** to 1.119 Å in **a1R-*R*-6a**) with a concomitant lengthening of the C–N bond of the product (*e.g.* from 1.394 to 1.462 Å in the *pro-R* route). Complexes **a1R-*R*-6a** and **a3S-*S*-6a** are stabilized as well by a hydrogen bond between the amido ligand and **6a** with N···H distances of 2.011 Å and 1.969 Å for **a1R-*R*-6a** and **a3S-*S*-6a**, respectively. The proton transfer step raises an important difference with the hydrogenation of acetophenone, as the deprotonation of the DPEN ligand by *N*-(phenyl)-1-phenylethylamide should be easier than that by 1-phenylethoxide, due to the higher basicity of the former. In addition, amido–amino complexes are significantly more stable than the parent ion pair species, with respective gains of free energy equal to 6.0 and 9.1 kcal mol^{-1} for **a1R-*R*-6a** and **a3S-*S*-6a**, respectively. It is worth noting in this context that the evolution of ionic pair species to the corresponding amido (or alkoxo complexes in ketone hydrogenation) is typically a very thermodynamically favorable step.[5h,33] In the present case, amido complex **N1R** is 4.2 kcal mol^{-1} lower in free energy than **ip-*pro-R***, although the magnitude of the stabilization is not as pronounced as reported for an *N*-(phenyl)phenylmethylamide compound.[33] Thus, **a1R-*R*-6a** is 1.8 kcal mol^{-1} more stable than **N1R** in free energy.[34]

Hydrogen activation. Although it has received less attention than the enantioselective reduction of the substrate, hydrogen activation constitutes a key mechanistic aspect in asymmetric hydrogenations performed by bifunctional catalysts. It is pertinent to note in this context that computational studies by Dub and Gordon about the hydrogenation of acetophenone catalyzed by *trans*-Ru(H)$_2$((*S*)-BINAP))((*S*,*S*)-DPEN) have shown that hydrogen activation by an ion pair species (assisted by the alkoxide fragment resulting from hydride transfer to the ketone) is a more favorable route than the direct activation by an amido–hydride complex.[5h] The involvement of the imine in the activation of hydrogen can therefore be a point of considerable interest in the present system that deserves study. Attending to the pathway described for the reduction of **5a** by **d1R**, hydrogen coordination and further activation by **a1R-*R*-6a** seems a plausible route for the second part of the catalytic cycle. Nevertheless, alternative pathways from ion pair **ip-*pro-R*** as well as direct activation by amido complex **a1R** have also been considered attending to aforementioned precedents.

Hydrogen interaction with **a1R-*R*-6a** started with a sequence of steps for H_2 coordination (Fig. 13). Approach of the H_2 molecule to the amido complex shows a first transition state (**TS3a**) with Ru–H distances of 2.812 and 2.662 Å, while the H–H distance in the complex is 0.749 Å, indicating a minimal interaction with the metal center (0.744 Å computed for free hydrogen). From **TS3a**, the reaction sequence first produces a loose dihydrogen complex **h1R-*R*-6a-l** (d(Ru–H) = 2.106, 2.160 Å, d(H–H) = 0.779 Å) and then a tight one **h1R-*R*-6a-t** characterized by shorter Ru–H distances of 1.779 and 1.746 Å and a H–H distance of 0.839 Å, as well as the corresponding transition state between them (**TS3b**). It is worthy to note that both dihydrogen complexes as well as transition states along the pathway are stabilized by a hydrogen bond to (*R*)-**6a**. **TS4a** connects the tight H_2 bound complex with a hydrogen bonded adduct between **d1R** and (*R*)-**6a** (**d1R-*R*-6a**). However, **TS4a** mainly shows proton

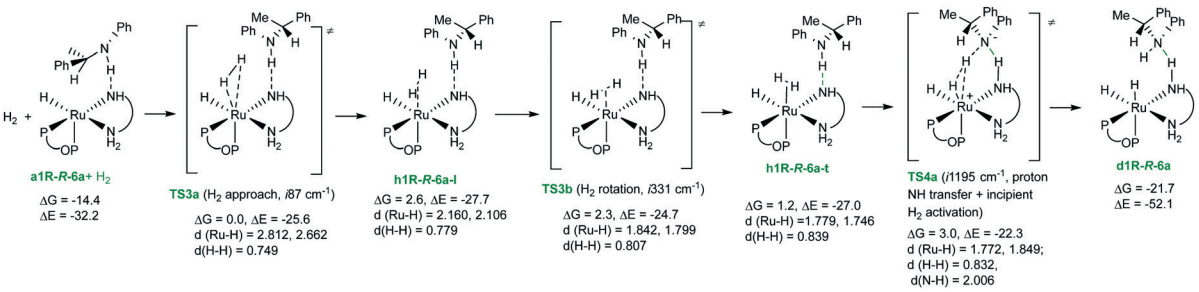

Fig. 13 Hydrogen activation by **a1R-*R*-6a** (ΔG and ΔE values in kcal mol^{-1} referenced to **a1R** + (*R*)-**6a** + H_2, bond distances in Å).

transfer from (*R*)-**6a** to the complex to generate an ionic-pair type species along with incipient activation of the coordinated H_2, assisted by deprotonated (*R*)-**6a**. Further activation of the coordinated H_2 is easy and IRC analysis from **TS4a** leads to **d1R-*R*-6a** in the product direction. It is worthy to note that the free energy of **TS4a** is only 1.8 kcal mol^{-1} above that of **h1R-*R*-6a-t**, indicating that ionization induced by the proton transfer step enables very easy hydrogen activation. Notwithstanding that, this is the step with the highest barrier in the coordination-activation of H_2 by **a1R-*R*-6a**.

Analysis of H_2 coordination to **ip-*pro-R*** led to a high energy transition state (**TS3c**, $\Delta G^{\ddagger}$ = 16.4 kcal mol^{-1}, Fig. 14). It seems that separation in toluene of the tightly bonded ionic components of the pair due to the uncompleted hydride transfer and the agostic interaction has a considerable energetic cost. **TS3c** shows a dissimilar interaction between Ru and both atoms of the H_2 molecule, with Ru–H distances of 2.161 and 2.548 Å, while the H–H distance (0.761 Å) indicates the scarce activation of dihydrogen. In addition, the N–H distances reflect the ionic-pair character of **TS3c**. Based on the comments made above, one might expect that H_2 is quite ready to be activated from **TS3c** and indeed, an IRC analysis from this transition state directly leads in the product direction to a hydrogen bonded adduct between (*R*)-**6a** and **d1R**, which differs from **d1R-*R*-6a** in the orientation of the amine.

A third possible H_2 activation pathway corresponds to non-assisted activation by amido complex **a1R**. Examination of the coordination of the hydrogen molecule to the **a1R** complex displayed an analogous pathway to that described for **a1R-*R*-6a**, with loose and tight H_2 complexes and corresponding transition states (see the ESI† for further details). Activation of the coordinated hydrogen in the tight complex **h1R-t** leads to **TS4b** ($\Delta G^{\ddagger}$ = 16.6 kcal mol^{-1}) and then to **d1R**. It is worthy to note that most of the energetic cost of the hydrogen activation process corresponds to the coordination of the H_2 molecule, since reaching the **h1R-t** species has an energetic cost of 12.1 kcal mol^{-1} with respect to **a1R** and H_2, while the subsequent step (**TS4b**) has a low relative $\Delta G^{\ddagger}$ value (4.5 kcal mol^{-1}) with respect to **h1R-t**. The comparison between the activation schemes by **a1R-*R*-6a** and **a1R** indicates hydrogen bond stabilization from (*R*)-**6a** along the pathway in the first case, leading to a more favorable hydrogen activation route. Moreover, loose interaction between **a1R** and (*R*)-**6a** in **a1R-*R*-6a** compared with ionic fragments in **ip-*pro-R*** enables easier H_2 coordination. Finally, an analysis of the reaction profile using the energetic span model[35] indicates that the turnover determining intermediate (TDI) is **a1R-*R*-6a**, while the turnover determining transition state (TDTS) is **TS4a**, with an energetic span (δE) of 17.5 kcal mol^{-1}, which is an affordable free energy barrier at room temperature.

Although the results described above point to hydrogen activation as the turnover-limiting step, it should be noticed that the determination of the lowest hydrogen activation route in the present system is an exceedingly difficult task. For instance, **a1R-*R*-6a** should easily exchange amine with its

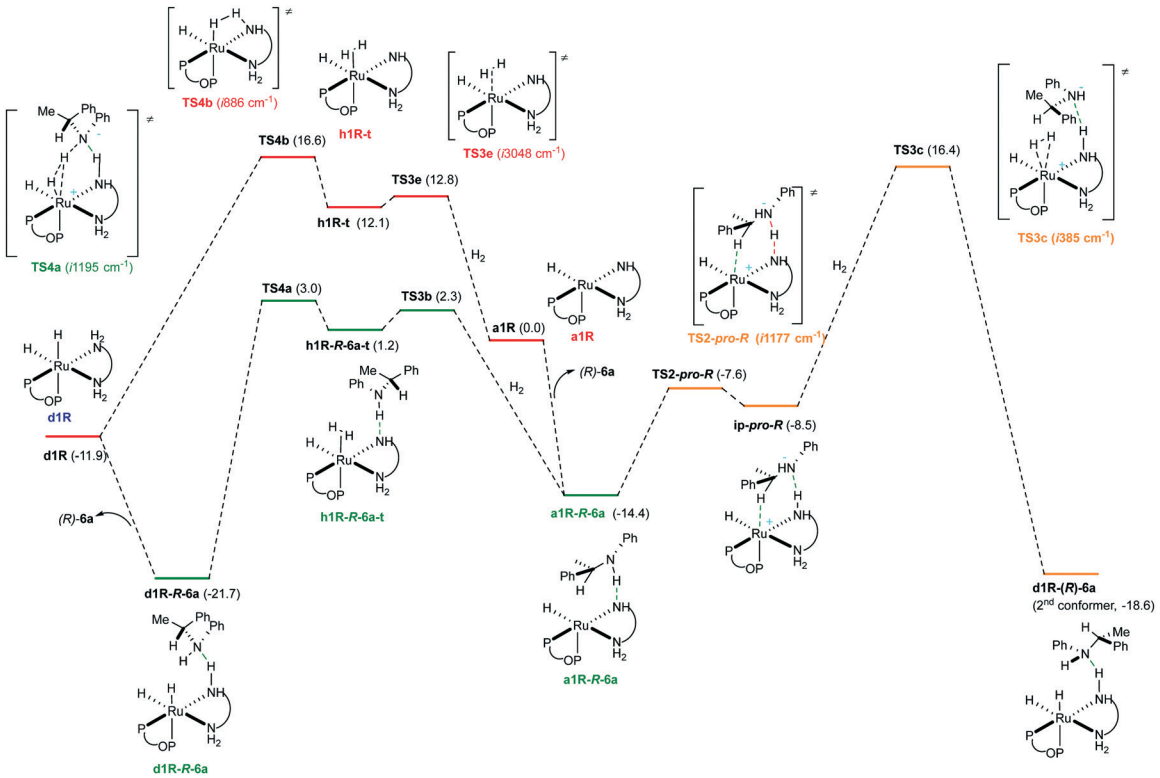

Fig. 14 General scheme for the hydrogen activation pathways. ΔG values in brackets in kcal mol^{-1} referred to **a1R** + (*R*)-**6a** + H_2.

S enantiomer. In addition, hydrogen bond interaction between **6a** and the amido complex generates a stereogenic center at nitrogen for which two configurations are possible resulting from easy nitrogen inversion in **6a**. In addition, proton transfer between amido and amino fragments of the DPEN ligand assisted by **6a** should also be a feasible step. As already mentioned, easy atropisomerization of the biaryl fragment in pentacoordinate amido complexes is an additional variable to consider. Recalling, finally, the fluxional nature described for $RuH(NHCMe_2CMe_2NH_2)(PPh_3)_2$[5a] and considering the existence of several amido–hydride complexes in a narrow interval of energy (Fig. 7), isomerization of **a1R** may be an additional factor to consider.

Product configuration and enantioselectivity. The irreversible formation of amine observed experimentally points to the hydride insertion as the enantiodetermining step.[36] Thus, the general scheme drawn for the reduction of **5a** explains the configuration of the amine product obtained experimentally (*i.e.* (*R*)-**6a** from **1a**). It is worthy to note that the chiral diamine induces a strong preference in product configuration. Thus, in addition to the favored formation of (*R*)-**6a** from **d1R**, *trans* dihydrides **dtR** and **dtS** also show a significant preference for (*R*)-**6a**, as the most favorable *pro-R* TS1 is 3.8 kcal mol^{-1} lower in free energy than the most favorable *pro-S* TS1 for the *trans* isomers. In contrast, metal configuration prevails in **d3S** over that of DPEN favouring the formation of (*S*)-**6a** (3.3 kcal mol^{-1} difference in free energy between most favourable *pro-S* and *pro-R* TS1).

There is extensive information in the literature about fluxionality and isomerization of ruthenium dihydrides.[37] Particularly relevant in this context, Morris has studied in detail the behavior of complex **A**, observing the isomerization between *trans*,*cis* and *cis*,*cis* isomers (with the latter being more stable),[5c] pointing to a non-dissociative trigonal twist mechanism for the exchange.[38] Due to the complexity introduced by the atropisomerization of the phosphine–phosphite ligand, we have not investigated the exchange between **d1R** and **d3S**, but considering that coincident enantioselectivities were obtained independent of the stereochemistry of $Ru(Cl)_2$(**2a**)(**3a**), such an exchange may also be operative in the present system. Following this assumption, the value of $\Delta\Delta G^{\ddagger}$ of 1.6 kcal mol^{-1} between **TS1-d1R-RP-5a** and **TS1-d3S-SP-5a** gives an estimation of 88% ee for the enantioselectivity, while the value of $\Delta\Delta E^{\ddagger}$ of 1.9 kcal mol^{-1} corresponds to 92% ee. Using a more extended basis set (def2QZVP for Ru and 6-311++g(2d,p) for main group atoms), a value of $\Delta\Delta E^{\ddagger}$ equal to 1.9 kcal mol^{-1} was obtained (91% ee). These values therefore show a good agreement with the experimental value of 94% ee. A remarkable difference between these transition states regards metal configuration.[39] Thus, in the case of **d1R**, there is a matched combination of diamine and metal configurations which enables a better fitting of the substrate in the pocket generated by the dihydride, therefore allowing a shorter N(imine)···HN hydrogen bond[40] in **TS1-d1R-RP-5a** than in **TS1-d3S-SP-5a**.

Despite the different backbones in dihydrides $Ru(H)_2$(**2a**)(**3a**) and $Ru(H)_2$(**2c**)(**3a**), a comparison between isomers of each type (*i.e.* **d1R**, **d3S**, **dtR** and **dtS** with **d1R′**, **d1S′**, **dtR″** and **dtS″**, respectively) shows rather coincident structures. In addition, from the Ru–H distances of the $Ru(H)_2$(**2c**)(**3a**) complexes, a comparable reactivity between *cis* and *trans* dihydrides can be expected. Based on these considerations, a pathway involving *cis*-dihydrides seems also plausible for catalysts with a phenylene backbone. However, as the stabilization of imine–dihydride precomplexes and corresponding TS1 depend on a precise substrate–complex recognition, this possibility cannot be ascertained without a detailed analysis of all possible pathways, which is further complicated by the conformational properties of the phosphine–phosphite ligand.

Conclusions

Complexes **1** have selectively been obtained as *trans* isomers by subsequent treatment of $RuCl_2(PPh_3)_3$ with P–OP and N–N ligands. In the case of **1a**, a clean *trans* to *cis* isomerization has been observed by heating in EtOH. DFT calculations performed with $Ru(Cl)_2$(**2a**)(**3a**) reproduce the higher stability of the *cis* isomers over the *trans* isomers as well as the low energy difference between atropisomers of *trans*-**1a** observed experimentally. Moreover, a strong bias on biaryl configuration caused by metal and diamine chirality is observed in *cis*-**1** and *cis*-**3** type isomers. Complexes **1** are effective catalyst precursors for the enantioselective hydrogenation of *N*-aryl imines **5** under very mild conditions with satisfactory enantioselectivities (84–96% ee, 16 examples). The catalyst performance is also suitable for multigram hydrogenation as shown in the case of the synthesis of **6h**. Complex $Ru(H)(BH_4)$(**2c**)(**3b**) hydrogenates **5a** in ^{i}PrOH without the need of an additional base, giving nearly coincident enantioselectivity with **1e** in ^{i}PrOH using 5 equiv. of base, pointing to a common enantiodetermining step in both reactions. Likewise, the enantioselectivity in the hydrogenation of **5g** under standard conditions did not depend on the stereochemistry of starting $Ru(Cl)_2$(**2a**)(**3a**), while additional experiments pointed to the irreversible reduction of this substrate.

In addition, the mechanism of the reduction of **5a** by $Ru(H)_2$(**2a**)(**3a**) has been calculated by DFT methods. Results obtained from the latter are in accord with a stepwise reduction of the imine,[41] with the hydride transfer being enantiodetermining, while the *pro-R* and the *pro-S* routes are generated by **d1R** and **d3S** dihydrides, respectively. Calculations rationalize the configuration of the preferred product enantiomer and show a good agreement with experimental enantioselectivity. From the examination of several hydrogen activation pathways, the most favourable one is initiated by hydrogen coordination to hydrogen bonded adduct **a1R-*R*-6a**, followed by activation of the η^2-H_2 assisted by the amine. In the latter, proton transference from the amine to the amido ligand, leading to an ion pair species, has been observed before an easy hydrogen activation step.

Conflicts of interest

There are no conflicts to declare.

Acknowledgements

This work was supported by the Spanish Ministry of Science and Innovation (projects CTQ2016-75193-P; AEI/FEDER, UE, RED2018-102387-T, PID2019-110856GA-I00 and PGC2018-100818-A-I00). The Mass Spectrometry Service of the Universidad de Sevilla (CITIUS) is acknowledged for technical assistance as well as the Supercomputing Center of Galicia (CESGA) for the access to computing facilities. Dr. Joaquín López-Serrano is also gratefully acknowledged for providing valuable comments. A. C.-V. also thanks the Spanish MEC and the European Social Fund (Ramón y Cajal Fellowship: RyC-2016-19930). We acknowledge support of the publication fee by the CSIC Open Access Publication Support Initiative through its Unit of Information Resources for Research (URICI). This work is dedicated to Prof. Antonio Otero on the occasion of his retirement.

Notes and references

1 For reviews on this topic, see: (*a*) R. Noyori and T. Ohkuma, *Angew. Chem., Int. Ed.*, 2001, **40**, 40; (*b*) S. E. Clapham, A. Hadzovic and R. H. Morris, *Coord. Chem. Rev.*, 2004, **248**, 2201; (*c*) M. Ito and T. Ikariya, *Chem. Commun.*, 2007, 5134.

2 (*a*) T. Ohkuma, H. Ooka, T. Ikariya and R. Noyori, *J. Am. Chem. Soc.*, 1995, **117**, 10417; (*b*) T. Ohkuma, H. Ooka, S. Hashiguchi, T. Ikariya and R. Noyori, *J. Am. Chem. Soc.*, 1995, **117**, 2675; (*c*) H. Doucet, T. Ohkuma, K. Murata, T. Yokozawa, M. Kozawa, E. Katayama, A. F. England, T. Ikariya and R. Noyori, *Angew. Chem., Int. Ed.*, 1998, **37**, 1703; (*d*) T. Ohkuma, M. Koizumi, H. Doucet, T. Pham, M. Kozawa, K. Murata, E. Katayama, T. Yokozawa, T. Ikariya and R. Noyori, *J. Am. Chem. Soc.*, 1998, **120**, 13529; (*e*) T. Ohkuma, D. Ishii, H. Takeno and R. Noyori, *J. Am. Chem. Soc.*, 2000, **122**, 6510; (*f*) T. Ohkuma, C. A. Sandoval, R. Srinivasan, Q. Lin, Y. Wei, K. Muñiz and R. Noyori, *J. Am. Chem. Soc.*, 2005, **127**, 8288.

3 (*a*) V. F. Kuznetsov, G. P. A. Yap and H. Alper, *Organometallics*, 2001, **20**, 1300; (*b*) Y. Xu, N. W. Alcock, G. J. Clarkson, G. Docherty, G. Woodward and M. Wills, *Org. Lett.*, 2004, **6**, 4105; (*c*) R. Guo, C. Elpelt, X. Chen, D. Song and R. H. Morris, *Chem. Commun.*, 2005, 3050; (*d*) Q. Jing, X. Zhang, J. Sun and K. Ding, *Adv. Synth. Catal.*, 2005, **347**, 1193; (*e*) W. Li, X. Sun, L. Zhou and G. Hou, *J. Org. Chem.*, 2009, **74**, 1397; (*f*) Y. Li, K. Ding and C. A. Sandoval, *Org. Lett.*, 2009, **11**, 907; (*g*) B. Stegink, L. van Boxtel, L. Lefort, A. J. Minnaard, B. L. Feringa and J. G. de Vries, *Adv. Synth. Catal.*, 2010, **352**, 2621; (*h*) Q. Zhu, D. Shi, C. Xia and H. Huang, *Chem. – Eur. J.*, 2011, **17**, 7760; (*i*) K. Matsumura, N. Arai, K. Hori, T. Saito, N. Sayo and T. Ohkuma, *J. Am. Chem. Soc.*, 2011, **133**, 10696.

4 (*a*) K. Abdur-Rashid, A. J. Lough and R. H. Morris, *Organometallics*, 2000, **19**, 2655; (*b*) C. J. Cobley and J. P. Henschke, *Adv. Synth. Catal.*, 2003, **345**, 195; (*c*) K. Abdur-Rashid, R. Guo, A. J. Lough, R. H. Morris and D. Song, *Adv. Synth. Catal.*, 2005, **347**, 571; (*d*) J.-H. Xie, Z.-T. Zhou, W.-L. Kong and Q.-L. Zhou, *J. Am. Chem. Soc.*, 2007, **129**, 1868; (*e*) T. Li, I. Bergner, F. N. Haque, M. Z. De Iuliis, D. Song and R. H. Morris, *Organometallics*, 2007, **26**, 5940; (*f*) J. M. John and S. H. Bergens, *Angew. Chem., Int. Ed.*, 2011, **50**, 10377.

5 (*a*) K. Abdur-Rashid, S. E. Clapham, A. Hadzovic, J. N. Harvey, A. J. Lough and R. H. Morris, *J. Am. Chem. Soc.*, 2002, **124**, 15104; (*b*) C. A. Sandoval, T. Ohkuma, K. Muñiz and R. Noyori, *J. Am. Chem. Soc.*, 2003, **125**, 13490; (*c*) R. Abbel, K. Abdur-Rashid, M. Faatz, A. Hadzovic, A. J. Lough and R. H. Morris, *J. Am. Chem. Soc.*, 2005, **127**, 1870; (*d*) A. Hadzovic, D. Song, C. M. MacLaughlin and R. H. Morris, *Organometallics*, 2007, **26**, 5987; (*e*) M. Z.-D. Iuliis and R. H. Morris, *J. Am. Chem. Soc.*, 2009, **131**, 11263; (*f*) A. Comas-Vives, G. Ujaque and A. Lledós, *Inner- and Outer-Sphere Hydrogenation Mechanisms: A Computational Perspective*, Elsevier Masson SAS, 2010, vol. 62; (*g*) F. Hasanayn and R. H. Morris, *Inorg. Chem.*, 2012, **51**, 10808; (*h*) P. A. Dub, N. J. Henson, R. L. Martin and J. C. Gordon, *J. Am. Chem. Soc.*, 2014, **136**, 3505; (*i*) P. A. Dub and J. C. Gordon, *Dalton Trans.*, 2016, **45**, 6756.

6 P. A. Dub and J. C. Gordon, *ACS Catal.*, 2017, **7**, 6635.

7 (*a*) D. S. Zerla, I. Rimoldi, E. Cesarotti, G. Facchetti, M. Pellizzoni and M. Fusè, *J. Organomet. Chem.*, 2014, **771**, 2; (*b*) T. Cruchter and V. A. Larionov, *Coord. Chem. Rev.*, 2018, **376**, 95.

8 N. Arai, N. Utsumi, Y. Matsumoto, K. Murata, K. Tsutsumi and T. Ohkuma, *Adv. Synth. Catal.*, 2012, **354**, 2089.

9 (*a*) W. Baratta, G. Chelucci, E. Herdtweck, S. Magnolia, K. Siega and P. Rigo, *Angew. Chem., Int. Ed.*, 2007, **46**, 7651; (*b*) F. Chen, D. He, L. Chen, X. Chang, D. Z. Wang, C. Xu and X. Xing, *ACS Catal.*, 2019, **9**, 5562.

10 (*a*) M. Vaquero, A. Suárez, S. Vargas, G. Bottari, E. Álvarez and A. Pizzano, *Chem. – Eur. J.*, 2012, **18**, 15586; (*b*) P. Kleman, M. Vaquero, I. Arribas, A. Suárez, E. Álvarez and A. Pizzano, *Tetrahedron: Asymmetry*, 2014, **25**, 744.

11 For examples of catalysts containing atropisomerizable phosphites, see: (*a*) G. J. H. Buisman, M. E. Martin, E. J. Vos, A. Klootwijk, P. C. J. Kamer and P. W. N. M. van Leeuwen, *Tetrahedron: Asymmetry*, 1995, **6**, 719; (*b*) S. Deerenberg, H. S. Schrekker, G. P. F. Van Strijdonck, P. C. J. Kamer, P. W. N. M. Van Leeuwen, J. Fraanje and K. Goubitz, *J. Org. Chem.*, 2000, **65**, 4810; (*c*) S. Deerenberg, O. Pàmies, M. Diéguez, C. Claver, P. C. J. Kamer and P. W. N. M. Van Leeuwen, *J. Org. Chem.*, 2001, **66**, 7626; (*d*) J. Mazuela, J. J. Verendel, M. Coll, B. Schäffner, A. Börner, P. G. Andersson, O. Pàmies and M. Diéguez, *J. Am. Chem. Soc.*, 2009, **131**, 12344.

12 (*a*) K. Mikami, T. Korenaga, M. Terada, T. Ohkuma, T. Pham and R. Noyori, *Angew. Chem., Int. Ed.*, 1999, **38**, 495; (*b*) K. Aikawa and K. Mikami, *Angew. Chem., Int. Ed.*, 2003, **42**, 5455; (*c*) K. Akiyama, K. Wakabayashi and K. Mikami, *Adv. Synth. Catal.*, 2005, **347**, 1569; (*d*) K. Mikami, H. Kakuno and K. Aikawa, *Angew. Chem., Int. Ed.*, 2005, **44**, 7257; (*e*) K. Mikami, K. Wakabayashi and K. Aikawa, *Org. Lett.*, 2006, **8**, 1517; (*f*) K. Mikami, K. Wakabayashi, Y. Yusa and K. Aikawa, *Chem. Commun.*, 2006, 2365; (*g*) K. Wakabayashi, K.

Aikawa, S. Kawauchi and K. Mikami, *J. Am. Chem. Soc.*, 2008, **130**, 5012.

13 For other examples of Ru complexes crystallized as mixture of diastereomers, see: (*a*) H. Brunner, M. Weber, M. Zabel and T. Zwack, *Angew. Chem., Int. Ed.*, 2003, **42**, 1859; (*b*) H. Brunner, T. Tsuno, M. Bodensteiner, S. Gärtner, C. Miyahara, S. Ito, T. Kurosawa and K. Koyama, *Eur. J. Inorg. Chem.*, 2016, **2016**, 5405.

14 For other examples, see: (*a*) M. D. Fryzuk, C. D. Montgomery and S. J. Rettig, *Organometallics*, 1991, **10**, 467; (*b*) P. Crochet, J. Gimeno, S. García-Granda and J. Borge, *Organometallics*, 2001, **20**, 4369.

15 (*a*) R. S. Rowland and R. Taylor, *J. Phys. Chem.*, 1996, **100**, 7384; (*b*) J. Reedijk, *Chem. Soc. Rev.*, 2013, **42**, 1776.

16 For other examples of phosphite complexes exhibiting fast atropisomerization, see: (*a*) G. J. H. Buisman, L. A. van der Veen, A. Klootwijk, W. G. J. de Lange, P. C. J. Kamer, P. W. N. M. van Leeuwen and D. Vogt, *Organometallics*, 1997, **16**, 2929; (*b*) S. Deerenberg, P. C. J. Kamer and P. W. N. M. Van Leeuwen, *Organometallics*, 2000, **19**, 2065; (*c*) A. Suarez, A. Pizzano, I. Fernandez and N. Khiar, *Tetrahedron: Asymmetry*, 2001, **12**, 633; (*d*) M. Rubio, A. Suarez, D. D. Río, A. Galindo, E. Álvarez and A. Pizzano, *Organometallics*, 2009, **28**, 547; (*e*) M. Jouffroy, D. Sémeril, D. Armspach and D. Matt, *Eur. J. Org. Chem.*, 2013, 6069.

17 E. de Julián, E. Menéndez-Pedregal, M. Claros, M. Vaquero, J. Díez, E. Lastra, P. Gamasa and A. Pizzano, *Org. Chem. Front.*, 2018, **5**, 841.

18 A. Chelouan, R. Recio, L. G. Borrego, E. Álvarez, N. Khiar and I. Fernández, *Org. Lett.*, 2016, **18**, 3258.

19 (*a*) T. Ohkuma, M. Koizumi, K. Muñiz, G. Hilt, C. Kabuto and R. Noyori, *J. Am. Chem. Soc.*, 2002, **124**, 6508; (*b*) C. A. Sandoval, Y. Yamaguchi, T. Ohkuma, K. Kato and R. Noyori, *Magn. Reson. Chem.*, 2006, **44**, 66.

20 For other hydride–borohydride ruthenium complexes, see: (*a*) R. Guo, R. H. Morris and D. Song, *J. Am. Chem. Soc.*, 2004, **127**, 516; (*b*) R. Guo, X. Chen, C. Elpelt, D. Song and R. H. Morris, *Org. Lett.*, 2005, **7**, 1757.

21 The synthesis of dihydrides of formula RuH_2(**2**)(**3a**) was attempted using procedures described in the literature for the synthesis of ruthenium hydrides (*e.g.* treatment with H_2 in the presence of a base or reaction with hydride reagents), obtaining complex reaction mixtures in all cases. Moreover, attempts to access chlorohydrides RuH(Cl)(**2**)(**3a**) failed as well due to phosphite decomposition under reaction conditions in the reaction of $RuH(Cl)(PPh_3)_3$ (ref. 3*c*) with phosphine–phosphite ligands.

22 (*a*) O. Pàmies, A. H. Éll, J. S. M. Samec, N. Hermanns and J. E. Bäckvall, *Tetrahedron Lett.*, 2002, **43**, 4699; (*b*) A. H. Ell, J. S. M. Samec, C. Brasse and J.-E. Backvall, *Chem. Commun.*, 2002, 1144.

23 Calculations were performed with the Gaussian 09 program, using the B3PW91 functional, with the SDD basis set for Ru and 6-31g(d,p) for main group atoms, including D3 dispersion corrections and the use of the SMD continuum solvent model. For the latter, toluene was used for all calculations as it is the solvent used in the catalytic reactions (see the ESI† for further details).

24 It should be recalled that two different mechanistic pathways have been proposed to explain the dependence of the concentration of base in the asymmetric hydrogenation of ketones (ref. 5*h*). In reactions prepared without an added base or with a low concentration of base, ketone reduction by $Ru(H)_2$(diphosphine)(diamine) is proposed. In contrast, under high base concentration, alkaline dihydride–amidate complexes resulting from deprotonation of the diamine ligand are proposed as the key reductive species. Considering the low amount of base used in the present reactions, we have assumed that the neutral dihydride $Ru(H)_2$(**2a**)(**3a**) should be the reducing species in reactions performed with **1a** in toluene.

25 (*a*) T. G. Appleton, H. C. Clark and L. E. Manzer, *Coord. Chem. Rev.*, 1973, **10**, 335; (*b*) B. J. Coe and S. J. Glenwright, *Coord. Chem. Rev.*, 2000, **203**, 5.

26 For studies considering non-covalent interactions in Noyori type catalysts, see: (*a*) C. A. Sandoval, Q. Shi, S. Liu and R. Noyori, *Chem. – Asian J.*, 2009, **4**, 1221; (*b*) R. Feng, A. Xiao, X. Zhang, Y. Tang and M. Lei, *Dalton Trans.*, 2013, **42**, 2130.

27 A. J. Neel, M. J. Hilton, M. S. Sigman and F. D. Toste, *Nature*, 2017, **543**, 637.

28 For studies illustrating the importance of dispersion interactions in metal catalyzed reactions, see: (*a*) E. Lyngvi, I. A. Sanhueza and F. Schoenebeck, *Organometallics*, 2015, **34**, 805; (*b*) A. A. Thomas, K. Speck, I. Kevlishvili, Z. Lu, P. Liu and S. L. Buchwald, *J. Am. Chem. Soc.*, 2018, **140**, 13976; (*c*) F. H. Zhang, F. J. Zhang, M. L. Li, J. H. Xie and Q. L. Zhou, *Nat. Catal.*, 2020, **3**, 621.

29 P. Dydio and J. N. H. Reek, *Chem. Sci.*, 2014, **5**, 2135.

30 Graphical representation of NCI interactions performed with Multiwfn software:T. Lu and F. Chen, *J. Comput. Chem.*, 2012, **33**, 580.

31 In this context, it should be mentioned that a key element in the catalytic transfer hydrogenation of imines by the Shvo catalyst is substrate activation by hydrogen bonding: (*a*) J. S. M. Samec, A. H. Ell and J. E. Backvall, *Chem. Commun.*, 2004, 2748; (*b*) C. P. Casey, G. A. Bikzhanova, Q. Cui and I. A. Guzei, *J. Am. Chem. Soc.*, 2005, **127**, 14062; (*c*) J. B. Aberg, J. S. M. Samec and J. E. Backvall, *Chem. Commun.*, 2006, 2771; (*d*) C. P. Casey, T. B. Clark and I. A. Guzei, *J. Am. Chem. Soc.*, 2007, **129**, 11821; (*e*) A. Comas-Vives, G. Ujaque and A. Lledós, *Organometallics*, 2007, **26**, 4135; (*f*) A. Comas-Vives, G. Ujaque and A. Lledós, *Organometallics*, 2008, **27**, 4854.

32 A detailed analysis of the hydride transfer step shows the participation of intermediate ion pair species **ag-*pro-R*** and **ag-*pro-S***, respectively, with Ru–H distances of 1.903 and 1.899 Å, respectively, while the C–H ones amount to 1.228 and 1.223 Å, respectively, displaying an uncompleted hydride transfer (see the ESI† for details).

33 M. Hernández-Juárez, J. López-Serrano, P. Lara, J. P. Morales-Cerón, M. Vaquero, E. Álvarez, V. Salazar and A. Suárez, *Chem. – Eur. J.*, 2015, **21**, 7540.

34 A considerable effort has been dedicated to find TS connecting **ip-*pro-R*** and **N1R** without success. From data obtained from reaction scan, a barrier of $\Delta E^{\ddagger}$ = 6.4 kcal mol^{-1} and $\Delta G^{\ddagger}$ = 4.0 kcal mol^{-1} over **ip-*pro-R*** could be estimated (see the ESI† for details).

35 (*a*) S. Kozuch and S. Shaik, *Acc. Chem. Res.*, 2011, **44**, 101; (*b*) A. Uhe, S. Kozuch and S. Shaik, *J. Comput. Chem.*, 2011, **32**, 978.

36 For examples of reactions in which the enantiodetermining step is followed by a turnover determining one, see: (*a*) J. T. Issenhuth, F. P. Notter, S. Dagorne, A. Dedieu and S. Bellemin-Laponnaz, *Eur. J. Inorg. Chem.*, 2010, 529; (*b*) J. S. Bandar, M. T. Pirnot and S. L. Buchwald, *J. Am. Chem. Soc.*, 2015, **137**, 14812.

37 (*a*) D. H. Gerlach, W. G. Peet and E. L. Muetterties, *J. Am. Chem. Soc.*, 1972, **94**, 4545; (*b*) P. Meakin, E. L. Muetterties and J. P. Jesson, *J. Am. Chem. Soc.*, 1973, **95**, 75; (*c*) D. G. Gusev and H. Berke, *Chem. Ber.*, 1996, **129**, 1143; (*d*) J. A. Ayllón, C. Gervaux, S. Sabo-Etienne and B. Chaudret, *Organometallics*, 1997, **16**, 2000; (*e*) C. Soubra, Y. Oishi, T. A. Albright and H. Fujimoto, *Inorg. Chem.*, 2001, **40**, 620; (*f*) D. Schott, C. J. Sleigh, J. P. Lowe, S. B. Duckett, R. J. Mawby and M. G. Partridge, *Inorg. Chem.*, 2002, **41**, 2960.

38 (*a*) A. Rodger and B. F. G. Johnson, *Inorg. Chem.*, 1988, **27**, 3061; (*b*) S. Li and M. B. Hall, *Organometallics*, 1999, **18**, 5682.

39 An analogous reaction scheme with *cis* dihydrides differing in metal configuration leading to opposite product enantiomers has been previously proposed by Morris[5c] to explain low enantioselectivities observed in the stoichiometric hydrogenation of acetophenone with a mixture of Δ-*cis*,*cis* and Λ-*cis*,*cis*-**A** dihydrides.

40 For other examples of transition states in bifunctional catalysis stabilized by hydrogen bonds, see: (*a*) J. F. Sonnenberg, K. Y. Wan, P. E. Sues and R. H. Morris, *ACS Catal.*, 2017, **7**, 316; (*b*) C. S. G. Seo, T. Tannoux, S. A. M. Smith, A. J. Lough and R. H. Morris, *J. Org. Chem.*, 2019, **84**, 12040.

41 For concerted imine reduction pathways, see:(*a*) M. Yamakawa, H. Ito and R. Noyori, *J. Am. Chem. Soc.*, 2000, **122**, 1466; (*b*) Ref. 4*e*.